# GREEN SYNTHESIS OF GOLD NANOPARTICLES USING *MENTHA SPICATA L.* AND ITS APPLICATION AS A CATALYST FOR OXIDATION NADH TO $NAD^+$

Rafah M. Thyab[1], Abass J. Attia[2], Mahmoud H. Hadwan[2], Asad M. Hadwan[3], Hawraa S. Al-Kawaz[4], Rawaa M. Mohammed[5], Ruaa A. Altaee[6]

[1]*Department of Chemistry, Faculty of Science, University of Kufa Najaf city 54001, Iraq, rafah9103@gmail.com (R.M.T.)*
[2]*Department of Chemistry, College of Science, University of Babylon Hilla City, Babylon Governorate, p.o. 51002, Iraq, abbaslafta2009@yahoo.com (A.J.A.); mahmoudhadwan@gmail.com (M.H.H.)*
[3]*College of Dentistry, University of Manara Al-Amarah 12218, Iraq, Asadhadwan95@gmail.com (A.M.H.)*
[4]*Department of Pathological Analysis, College of Science, Al-Qasim Green University Hilla City 5101, Iraq, hawraa.saad@science.uoqasim.edu.iq (H.S.A.)*
[5]*Department of Medical Laboratories Techniques Al-Mustaqbal University College, Babylon, Iraq, rawaamagid@uomus.edu.iq (R.M.M.)*
[6]*College of Pharmacy, Al-Zahraa University for Women Karbala Governorate 11118, Iraq, ruaa.ali@alzahraa.edu.iq (R.A.A.)*

*Received 03 April 2025*
*Accepted 26 July 2025*
*DOI: 10.59957/jctm.v61.i3.2026.5*

## ABSTRACT

*Due to their high biocompatibility, stability, and unique characteristics, gold nanoparticles (AuNPs) have numerous applications in the medical and biological fields. Plant-based nanoparticle synthesis is beneficial over other biological processes because it can be scaled up to an industrial scale. The electrochemical measurement of dihydronicotinamide adenine dinucleotide (NADH) is crucial because it serves as a required coenzyme for several dehydrogenases. NADH is the final electron donor molecule in the mitochondrial electron transport pathway. This study examined the catalytic role of AuNPs produced using Mentha spicata L. in the oxidation of NADH to nicotinamide adenine dinucleotide ($NAD^+$). AuNPs reduced NADH fluorescence intensity. As the quantity of AuNPs increased, the intensity of the 260 nm $NAD^+$ band increased, while that of the 340 nm NADH band decreased. The surface plasmon absorbance band of AuNPs at 520 nm increased in intensity due to the presence of NADH. This study provides significant evidence that the AuNPs surface catalyzes the oxidation of NADH to $NAD^+$. The catalyst characteristic of this crucial reaction may have significant potential applications in the biological and medicinal fields.*

Keywords: *nanotechnology, fluorescence, nicotinamide adenine dinucleotide, gold nanoparticles, antioxidant.*

## INTRODUCTION

Researchers have devoted considerable time and effort to studying nanotechnology in recent years [1]. The characteristics of nanomaterials differ significantly from those of their bulk counterparts. Recent techniques focus on low-cost alternatives for producing and manipulating nanoscale materials [2]. When it comes to advancing science and technology, nanotechnology is at the forefront [3].

Dihydronicotinamide adenine dinucleotide (NADH), tryptophan, pyridoxine, and riboflavin are some of the many fluorophores found in living cells, each stimulating and emitting light at a slightly different frequency [4]. Any metabolic shift in a cell population or activity can be traced back to a change in the quantities of these intracellular chemicals, which play crucial roles in cell growth and metabolism. Therefore, many critical

physiological factors of a fermentation process can be monitored in real time via fluorescence detection of cell fluid at various stimulation frequencies using non-invasive optical sensors. Since fluorescence readings are visual, there is no latency associated with acquiring and tracking this vital information about cells' internal processes [5].

The two primary intracellular electron transporters in living organisms are nicotinamide adenine dinucleotide ($NAD^+$) and NADH. More than 300 different dehydrogenase enzymes require $NAD^+$ as a coenzyme. In living cells, reversible redox reactions involve nicotinamide adenine dinucleotide (NAD) molecules. The two types of coenzymes are unphosphorylated $NAD^+$ and $NADP^+$. The reduced versions of $NAD^+$ and $NADP^+$ are NADH and NADPH, respectively. While NADH and NADPH give electrons to other compounds, $NAD^+$ and $NADP^+$ receive them. The microconidial transport chain is a multi-enzyme redox system in which NADH serves as a central component [6].

To detect fluorescence in a culture, a specific frequency of light must first excite a specific molecule within the cells. A photodiode or photomultiplier detects the slightly longer wavelength of light emitted by the stimulated fluorophore. When cells are illuminated at 366 nm, NADPH fluoresces at 460 nm. This trait has been heavily examined to gain insights into how alterations in cultural behaviour affect the amounts of reduced pyridine nucleotides. NADH fluorescence has been shown to represent the internal milieu of bacteria colonies subjectively and numerically [7].

*Mentha spicata L.* (spearmint) is a versatile herb with diverse antioxidant, pharmacological, and biological properties. Due to its pharmacological and biological properties, *M. spicata L.* is used in traditional medicine. Its phenolic acids, flavonoids, and terpenes have antioxidant, anti-inflammatory, analgesic, and antibacterial activities. Phenolic chemicals in *M. spicata L.* scavenge free radicals and prevent oxidative stress, protecting cells [8, 9]. *M. spicata L.* has been found to have anti-diabetic effects, with studies demonstrating that it can reduce blood glucose levels and enhance insulin sensitivity. Additionally, M. spicata L. has been found to possess anti-inflammatory properties, with its essential oil exhibiting anti-inflammatory effects in animal models [10, 11].

Metal nanoparticles play a crucial role in redox reactions due to their unique properties and high reactivity. The efficient transfer of electrons between reactants is crucial for numerous biological and industrial processes, and metal nanoparticles provide a promising approach to enhancing their efficiency and selectivity [12]. Continuing research in this field focuses on developing new metal nanoparticles with tailored properties for specific redox reactions and enhancing our understanding of the fundamental mechanisms underlying their catalytic activity [13, 14]. Metallic nanoparticles are appealing catalysts due to their high surface-to-volume ratio and increased surface atomic catalytic activity compared to mass materials.

This study employs UV-Vis absorbance and fluorescence spectroscopy to investigate the effects of gold nanoparticles (AuNPs) on NADH in detail. AuNPs were found to actively affect the oxidation of NADH to $NAD^+$, an essential biological process. The catalytic ability of AuNPs in the oxidation-reduction of NADH could be beneficial for future metabolic and medicinal applications.

## EXPERIMENTAL

### Materials

β-Nicotinamide adenine dinucleotide sodium salt (NADH-$Na_2$), chloroauric acid, and 2,2-diphenyl-1-picrylhydrazyl hydrate (DPPH) were purchased from Sigma-Aldrich Chemicals.

### Preparation of plant extract and synthesis of AuNPs

Leaves of Iraqi Mentha spicata L. were cut into small pieces and diced in a blade blender, and 5 g of leaves were heated with a stirrer at 50 - 70ºC with 100 mL of double distilled water (DDW) and twice with 70 % methanol for 15 min. It was filtered using Whatman No. 1 filter paper and stored in the freezer. The synthesis of AuNPs was performed by reducing one mM or 1.0 g $L^{-1}$ of chloroauric acid (10 mL) with 750 µL of leaf extract at 70°C. Slight heating for several minutes was required until GNP formation was observed, as indicated by the color change to a deep red or purple in the gold nanoparticle product's colour indicator.

### Purification of AuNPs

The phyto-reduced sample will aggregate after acetone (1:4) treatment, but cold spinning may separate

it and disperse the particles. The resultant pellet was cleaned and dissolved in sterile deionized water to produce biochemically inert nanoparticles.

**Characterization of AuNPs**

***UV-Vis spectral analysis***

The UV-Vis spectrum of the reaction solution was measured after diluting a small amount with deionized water, yielding a spectrum over a broad range of 200 to 800 nm. This permitted the monitoring of the reduction of purified gold ions.

**The free radical scavenging activity (2,2-Diphenyl-1-picrylhydrazyl (DPPH) assay)**

By applying the DPPH assay, it was determined the extent to which AuNPs were able to capture the steady free radical [15, 16]. In a nutshell, DPPH was dissolved in methanol at a concentration of 0.1 mM. To 3 mL of methanolic DPPH solution, we added a portion of AuNPs (20 - 100 µL). The absence of AuNPs was used as a negative control, and methanol with DPPH was used as a positive control. After 30 min of incubation, the radical scavenging activity was determined by measuring the degree to which the purple hue had faded at an absorbance of 517 nm. Free radical scavenging activity was calculated as follows: FRSA= [(*A*c - *A*s)/*A*c] × 100. After 60 min, compare the absorption of the material under test (As) to that of the reference (Ac).

**Cupric reducing antioxidant capacity (CUPRAC)**

The antioxidants in the sample or standard act to reduce $Cu^{++}$ to $Cu^{+}$. This reduced copper will create a 2:1 combination with the chromogenic substance in a highly selective method [17]. The most excellent absorbance of this constant compound develops at 450 nm. The results from each sample are compared to those from a reference solution containing a known quantity of Trolox.

**NADH fluorescence inhibition**

A simple mixing of standard gold solutions (OD = 1.0) and stock NADH solutions (0.03 - 0.9 mL) with water was used to create a final solution in a total volume of 3.0 mL, resulting in a series of combined solutions of AuNPs and NADH. According to Stephan Link's calculation of the absorption coefficient ($\varepsilon = 7.2 \times 10^8$ for gold nanoparticles smaller than 15 nm), the end quantities of gold nanoparticles were determined [18].

**NADH absorbance inhibition**

The absorbance spectrum of each sample was recorded in a quartz cell using a Shimadzu UV-1801PC spectrophotometer. A Shimadzu RF-5301PC Spectro fluorophotometer was used to analyse the fluorescence spectrum at an excitation wavelength of 325 nm.

## RESULTS AND DISCUSSION

**AuNP synthesis and characterization**

**UV spectrophotometry**

After adding *Mentha spicata L.*, the bioreduction of $Au^{3+}$ to $Au^{0}$ proceeds progressively. The leaf extract was mixed with chloroauric acid ($HAuCl_4$). The bio-reduced gold glyconanoparticles produced a purple-coloured solution, a characteristic of AuNPs [19]. This finding demonstrates an environmentally friendly method for stabilizing the created AuNPs and reducing the amount of gold ions. An example of the UV-Vis absorbance bands of *Mentha spicata L.*-derived AuNPs is shown in Fig 1.

Noble metal nanoparticles, such as silver and gold, exhibit surface plasmon resonance (SPR) bands with distinct absorbance peaks in the visible spectrum, making them crucial for various optical applications. Since nanoparticles lack metallic or atomic electrical characteristics due to their confined energy levels, the SPR band results from the quantum size effect of the nanoparticles. The size, inter-particle spacing, shielding type, and form of the nanoparticles significantly influence their electrical characteristics. A quantum size effect is observed when the de Broglie wavelength of the valence electrons has the same scale as the size of the atom itself. When this occurs, electrons act electrically like quantum spots in zero dimensions. In these metal containers, freely moving electrons become confined and exhibit the SPR band, a distinctive group vibration frequency of their plasma resonance.

Fig. 1 illustrates that the SPR band for AuNPs is located between 500 and 600 nm, and its position is closely related to the size of the nanoparticles. AuNPs smaller than 5 nm are challenging to identify and produce broad peaks in their SPR bands. However, the SPR band becomes more visible once particle size surpasses 5 nm. The SPR band shifts to shorter wavelengths for smaller nanoparticles, known as a blueshift, and to longer wavelengths for larger nanoparticles, known as a redshift.

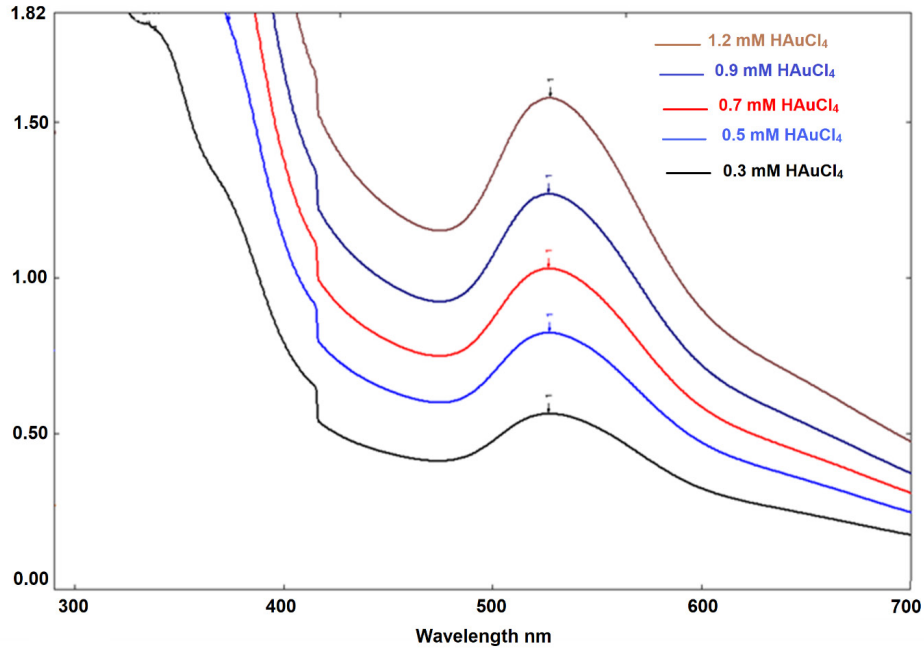


Fig. 1. The UV-Vis absorbance bands of AuNPs prepared from an extract of *Mentha spicata L*. The concentrations of AuNPs were varied from 1.2 mM to 0.3 mM.

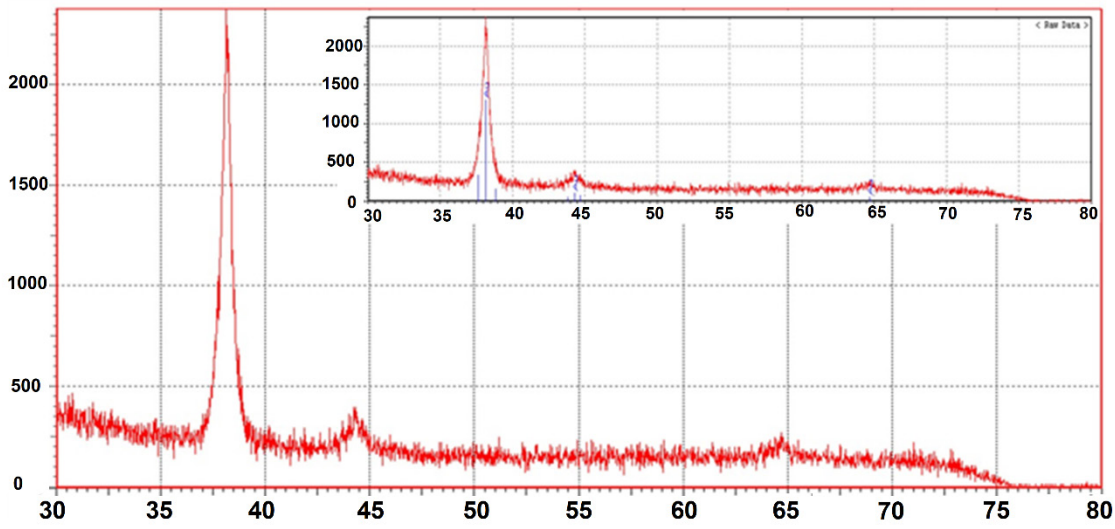


Fig. 2. The XRD pattern for gold nanoparticles synthesized by using *Mentha spicata L.* extract.

**X-ray diffraction (XRD)**

This study utilized a Phillips PW1830 diffractometer to investigate the XRD patterns of AuNPs synthesized via the bioreduction pathway at 40 kV and 20 mA with Cu Kα radiation. Fig. 2 shows the identified patterns.

The synthetic AuNPs' crystalline characteristic based on a face-centered cubic (fcc) structure was confirmed by an XRD pattern showing four diffraction peaks at 2θ values of 39.01°, 46.48°, 64.69°, and 77.62°. Scherer's calculation of the Bragg angle was used to determine that the average particle size of the produced AuNPs was 24 nm. The acquired XRD patterns confirmed the presence of gold colloids in the material. Like the report of the Joint Committee on

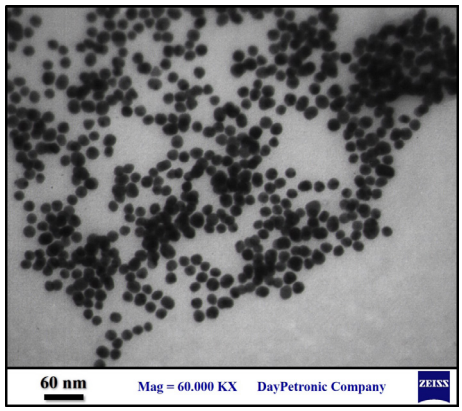


Fig. 3. TEM image for gold nanoparticles synthesized by using *Mentha spicata L.* extract.

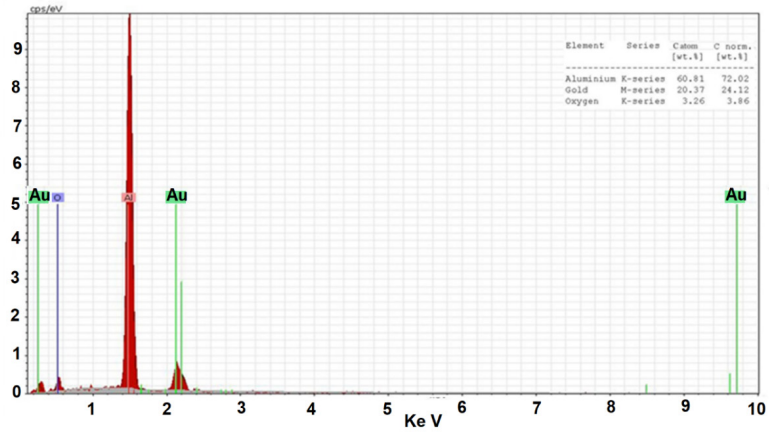


Fig. 4. EDX spectrum for gold nanoparticles synthesized by using *Mentha spicata L.* extract.

Particle Diffraction Standards (file no.: 04-0784) [20, 21], four distinct diffraction peaks-coded (111), (200), (220), and (311)-were found in the 2θ range of 20-80°, reflecting the fcc structure of solid gold. In addition, the XRD pattern showed a single, prominent diffraction point at 2θ = 39.01, corresponding to the (111) reflection of gold's fcc crystal structure. The (200), (220), and (311) reflection lines correspond to the 46.48°, 64.69°, and 77.62° weak diffraction peaks. The XRD results showed that the freshly created product comprised highly crystalline AuNPs. The resulting AuNPs had a particle size range of 11 - 77 nm, were monodisperse, and were spread evenly without aggregation.

**Transmission Electron Microscopy (TEM)**

TEM was used to probe the AuNPs' morphology. Fig. 3 shows a TEM image of the AuNPs, and Fig. 4 shows the energy-dispersive X-ray (EDX) spectrum of the AuNPs. A carbon-coated copper grid was used to prepare thin films of the sample; the grid was then placed under a suitable lamp for 5 min to dry the film after the excess solution had been blotted off with paper.

The TEM and EDX results of a typical AuNP sample indicate the large quantity and good uniformity achieved using this approach. These AuNPs had a mean diameter of 15 nm. The TEM image showed crystalline clusters and homogeneous solid AuNPs (Fig. 3). A nanomaterial's molecular composition can be determined using energy dispersive spectroscopy (EDX) [22]. EDX confirmed the creation of AuNPs, showing the highest count per second at 2.3 keV (Fig. 4).

**Dynamic light scattering (DLS)**

DLS is one of the most common methods for determining particle size, and its findings are shown in Fig. 5. When a homogeneous light beam, such as a laser, is shone onto a solution containing circular particles in Brownian motion, it undergoes a Doppler shift, altering the frequency of the oncoming light. The particle's size causes this variation. DLS enabled us to calculate the sphere size distribution and describe the AuNPs' movements in the medium by quantifying their diffusion coefficient and using the autocorrelation function.

An experiment was conducted using an advanced DLS system (Zetasizer Nano S, Malvern Instruments, UK). The distinctive peaks in the Zetasizer image (Fig. 5), which show an average diameter of 25 nm with extremely smooth borders, provide further evidence and confirmation of the biosynthesized gold nanostructure.

The AuNPs' zeta potential and particle size were measured using a Zetasizer instrument for further analysis. Fig. 5 shows that the typical AuNP had a diameter of around 25 nm and a zeta potential of -26.8 mV. The zeta potential showed the durability of colloidal gold in solution. A previous study reported that the ideal difference between a stable and unstable colloidal

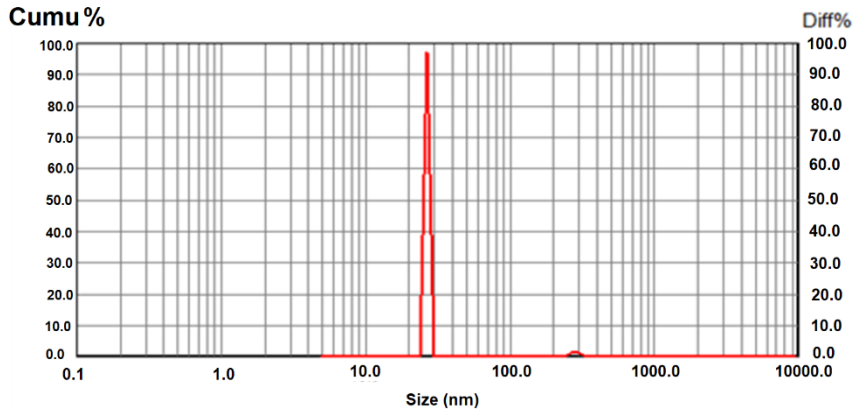


| Diam nm | Percent |
|---|---|
| 25.0 | 0.00 |
| 33.9 | 97.19 |
| 46.2 | 97.19 |
| 62.8 | 97.19 |
| 85.4 | 97.19 |
| 116 | 97.19 |
| 157 | 97.19 |
| 214 | 97.19 |
| 291 | 98.78 |
| 397 | 100.00 |

Fig. 5. Dynamic light scattering (DLS) of the gold nanoparticles produced by using *Mentha spicata L.* extract.

solution is typically greater than +30 mV or less than -30 mV. Stable particles often have zeta potentials > +30 mV or < -30 mV [23].

**Atomic force microscopy (AFM)**

Fig. 6 shows an atomic force micrograph of the synthesized AuNPs with aerial and 3D topographical views of the topological structures. The AFM images were also used to analyse the fractal behaviour of the placed and heated sheets. The AFM images were analysed to determine the porosity, irregularity, and fractal dimension. The surface shape was irregular due to both free and aggregated AuNPs.

**Cupric reducing antioxidant capacity (CUPRAC)**

Neocuproine copper(II) chloride, a novel reagent for the CUPRAC total antioxidant capacity test, is readily available, potent, selective, and responsive to all antioxidants [24]. CUPRAC was used to evaluate the antioxidant potential of three AuNP concentrations. Table 1 compares the $Cu^{2+}$-reducing ability of synthetic AuNPs with Trolox, a common antioxidant. Because the AuNPs reduced the Cu (II)-neocuproine reagent with a proportional change in their scavenging capacity, CUPRAC levels increased with the AuNP concentration (Table 1). The antioxidant test results demonstrated the effectiveness of AuNPs on various in vitro systems.

**2,2 - Diphenyl-1-picrylhydrazyl (DPPH) radical scavenging activity**

The colour of DPPH, a stable nitrogen-centered free radical, changes from violet to yellow when it is reduced via hydrogen reduction or electron transfer. Antioxidants, also known as radical scavengers, can cause this response [25]. The radical scavenging activity of all AuNPs under investigation increased with their concentration, demonstrating a concentration-dependent effect.

Most AuNPs used in biological applications today are groups shielded by polyheterofunctionalized monolayers. The mixed monolayer primarily comprises ligands that provide cluster stability and solubility in the aqueous medium, as well as ligands with biological functions (e.g., DNA, proteins, drugs, and biotic factors), and ligands that target specific directions (e.g., leading peptides, molecular ligands, and antibodies) [26].

AuNPs exhibit antioxidant activity due to their distinct physical characteristics, including a high surface-to-volume ratio and the ability to interact with biological molecules. They can scavenge free radicals, highly volatile chemicals that can harm cells and tissues through oxidative stress [27]. AuNPs have been shown to enhance the activity of antioxidant enzymes such as catalase and superoxide dismutase and encourage the production of antioxidant compounds, including glutathione and vitamin C [28]. Their form, size, and surface charge have a significant impact on their antioxidant activity. Because of their small size, AuNPs can enter cells and interact with cellular components. Additionally, because of their surface charge and functional groups, they can interact with proteins and effectively neutralize free radicals. Due to their unique characteristics, AuNPs are a promising antioxidant in various fields, including medicine, skincare, and the food industry [29, 30].

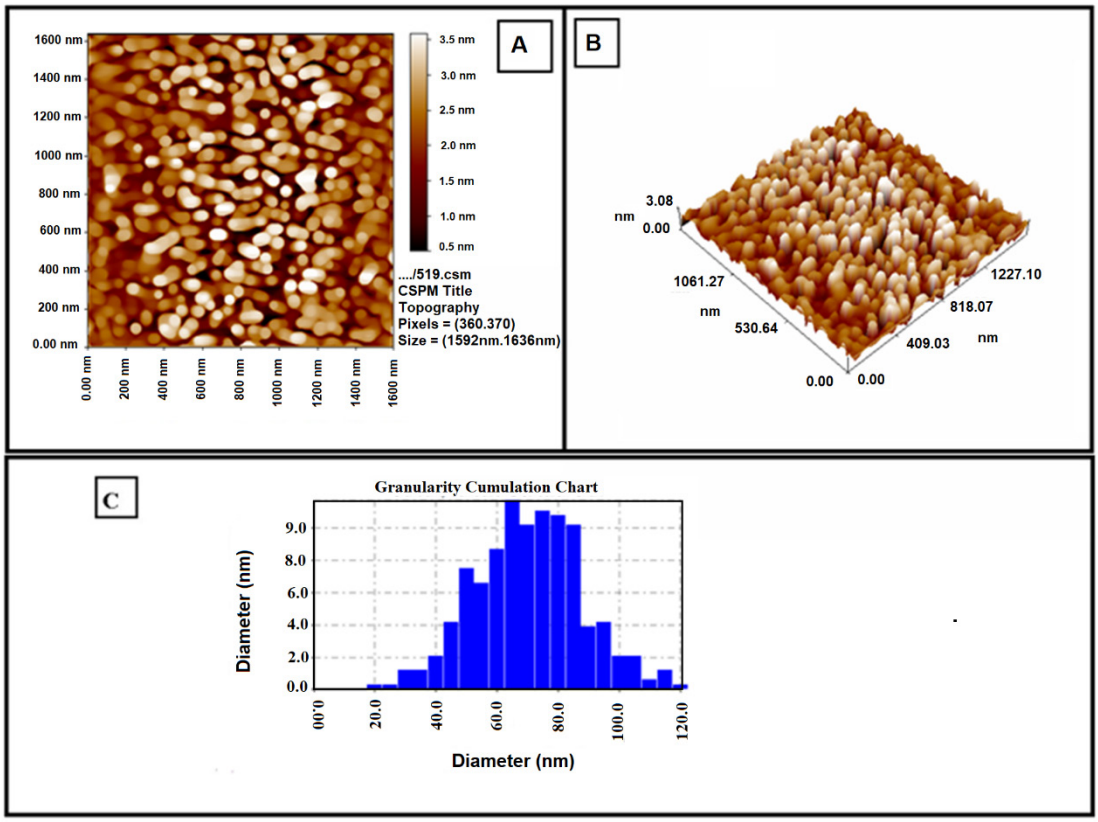


Fig. 6. AFM images of the gold synthesized nanoparticles by using *Mentha spicata L.* extract: (a) Topographic view, (b) Three-dimensional view and (c) distribution of particle diameters derived from.

Table 1. *In vitro* antioxidant assay of AgNPs by DPPH and CUPRAC methods (all values were measured as Trolox equivalent).

| Method / AuNPs concentration | DPPH Free Radical Scavenging method (Trolox equivalent, µmol $L^{-1}$) | CUPRAC Assay (Trolox equivalent, µmol $L^{-1}$) |
|---|---|---|
| 50 µmol $mL^{-1}$ | 155 | 245 |
| 100 µmol $mL^{-1}$ | 285 | 393 |
| 150 µmol $mL^{-1}$ | 390 | 545 |

**AuNP fluorescence properties**

AuNPs can quench the fluorescence of NADH, a coenzyme involved in various metabolic processes in living cells. When different AuNP concentrations were added to an NADH solution, NADH fluorescence decreased (Fig. 7). Adding AuNPs to the NADH solution effectively suppressed NADH's peak fluorescence at 460 nm (EX= 325 nm). The quenching effect increased with the concentration of AuNPs. The same reduction was seen at different NADH concentrations.

The fluorescence quenching of NADH by AuNPs was attributed to an interaction between the AuNP and the aromatic ring of the adenine moiety in NADH. This interaction leads to the transfer of electrons from the excited state of NADH to the AuNPs, resulting in a reduction in NADH fluorescence intensity. This

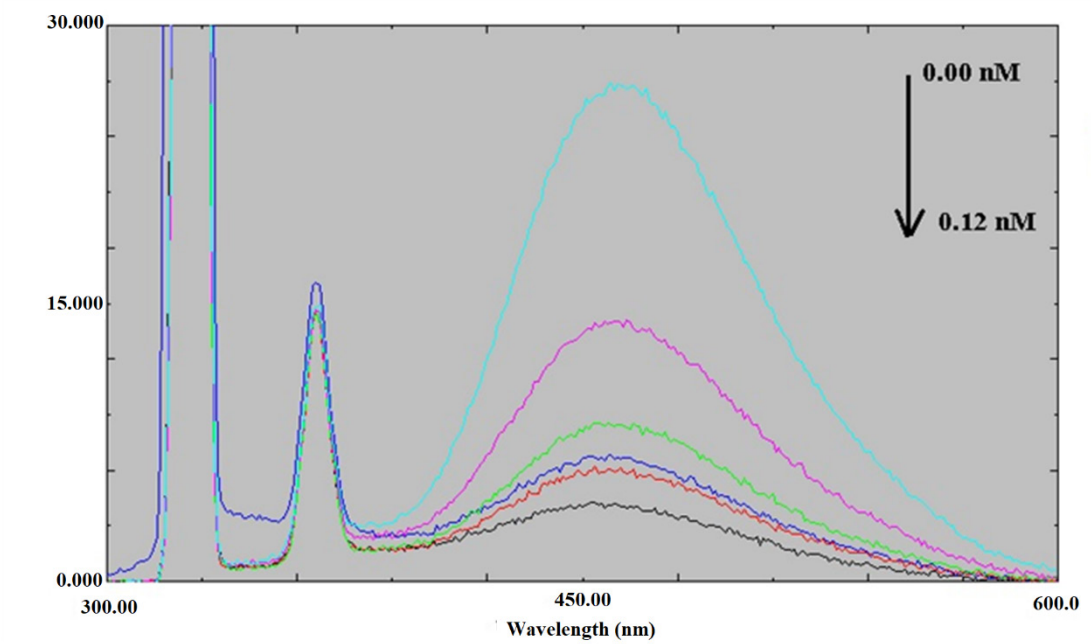


Fig. 7. NADH (0.08 mM) fluorescence spectroscopy at different concentrations of AuNPs (EX= 325 nm). The time-resolved fluorescence decay spectra of NADH at 460 nm, obtained at various gold nanoparticle quantities, are shown in the inset.

phenomenon has been studied in various contexts, including *in vitro* experiments and living cells, and has been utilized in the development of biosensors for measuring NADH [31]. The AuNPs' quenching effect on NADH fluorescence can be influenced by factors such as their size and shape, the distance between the AuNPs and NADH, and the concentrations of AuNPs and NADH [32]. The interaction between AuNPs and NADH offers a valuable tool for detecting and monitoring NADH-related metabolic processes in living cells, with potential applications in various fields, including medicine and biotechnology [33, 34]. For example, by using AuNPs to quench NADH fluorescence, biosensors could be designed to detect changes in NADH concentrations in biological samples. This approach has potential applications in fields such as clinical diagnosis and monitoring of metabolic disorders [35]. Another application of this interaction is in the imaging of living cells and tissues. The quenching effect of AuNPs on NADH fluorescence can be utilized to image NADH-related metabolic processes in living cells and tissues [36]. This approach has potential applications in fields such as cancer diagnosis and the monitoring of cellular metabolism [37]. Furthermore, the interaction between AuNPs and NADH can be utilized to investigate the mechanism of action of enzymes involved in NADH-related metabolic pathways, providing insights into their roles in cellular metabolism [22, 38].

**AuNP absorption properties**

The absorption spectra were recorded after adding AuNPs to the NADH solution. Fig. 8 shows NADH's three UV-Vis absorption bands. When the dihydronicotinamide moiety is in a coplanar conformation with the carboxamide moiety, electrons are conjugated between them, resulting in a band at 340 nm [38]. The adenine ring's π-π* shift is responsible for the stronger band at 260 nm. The dihydronicotinamide transition π-π* is responsible for the most substantial band at 205 nm. Fig. 8 shows that the NADH (260 nm) and AuNP (520 nm) absorption intensities increased linearly with AuNP concentration, while the 340 nm band intensity decreased. While the increase in the adenine ring's absorbance at 260 nm indicates that the AuNPs do not destroy the adenine, this band has a higher extinction coefficient than NADH. Due to the addition of $NAD^+$, the oxidized form of NADH, it has been noted that the 260 nm absorption coefficient of $NAD^+$ is higher than that of NADH ($14.4 \times 10^{-3}$). Due to a twisted and cisoid shape between the oxidized nicotinamide and carboxamide, the 340 nm band disappears [18]. Because $NAD^+$ has a more significant molar absorption coefficient

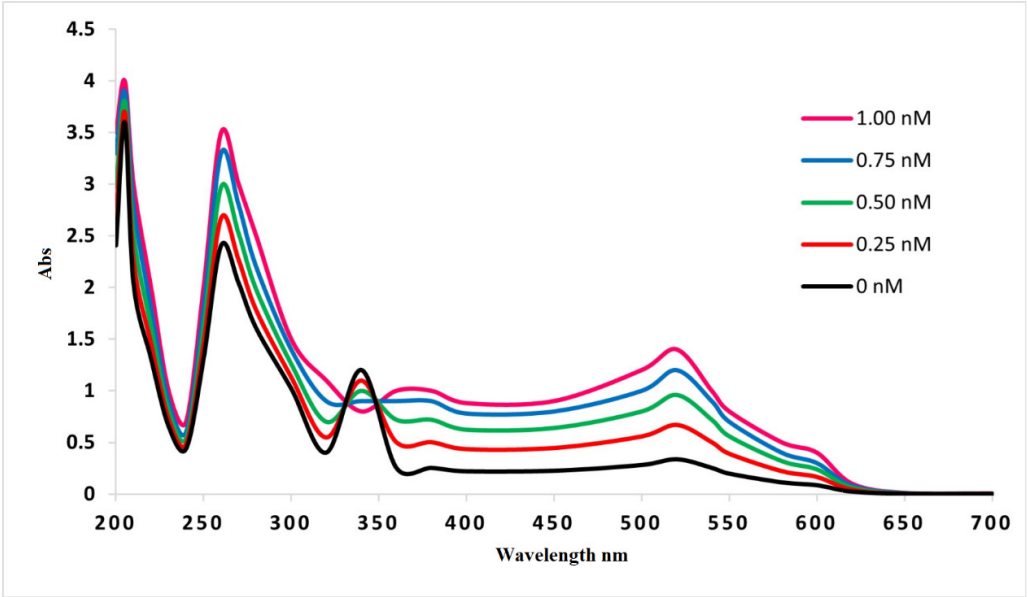


Fig. 8. Absorption spectrum bands of different concentrations of NADH (0.08 mM) and different concentrations of gold nanoparticles.

than NADH, the generation of $NAD^+$ may be what caused the rise in the 260 nm band and the drop in the 340 nm band. Due to the influence of Au nanoparticles, NADH's absorbance bands have changed, suggesting that NADH may be converted to $NAD^+$.

## CONCLUSIONS

Gold nanoparticles can affect the absorption and fluorescence spectra of nicotinamide adenine dinucleotide (NADH). When NADH molecules are close to gold nanoparticles, they can experience changes in their electronic environment, resulting in alterations to their absorption spectrum. This effect is thought to be due to the interaction between the NADH molecule and the AuNPs surface, which can alter the electronic structure of the molecule and result in a change in its absorbance properties. Additionally, the size and shape of the gold nanoparticles can also influence the magnitude and direction of this effect. For example, smaller nanoparticles have been found to have a more significant effect on the NADH absorption spectrum compared to larger nanoparticles. Overall, the effect of gold nanoparticles on the NADH absorption spectrum is an active area of research with potential applications in biosensing and imaging.

***Acknowledgments***

*The authors thank the presidency of the University of Babylon (Iraq) for its financial support, which made it possible to finish the protocol. The authors would also like to thank the Dean of the College of Science and the Head of the Chemistry Department at the University of Babylon, Iraq, for their assistance and support in completing the study.*

***Authors' contributions***

*R.M.T. , A.J.A., M.H.H., H.S.A., R.M.M.: Experimental work, Writing; M.H.H., A.M.H., R.A.T.: Experimental work, Review, editing; A.J.A., M.H.H., A.J.A.: Conceptualization, Design of the research, Editing of the manuscript, Project management, and funding acquisition.*

## REFERENCES

1. I.D. Muhammad, A comparative study of research and development related to nanotechnology in Egypt, Nigeria and South Africa, Technol. Soc., 68, 2022, 101888.

2. Y. Chen, X. Feng, Gold nanoparticles for skin drug delivery, Int. J. Pharm., 2022, 122122.
3. P. Singh, M. K. Tripathi, D. Kumar, Nanotechnology in Venom Research: Recent Trends and Its Application, Nanotechnol. Biomed. Appl., 2022, 381-389.
4. V. Caligiuri, F. Leone, F. Annesi, A. Pane, R. Bartolino, A. De Luca, Envisioning Quantum Electrodynamic Frameworks Based on Bio-Photonic Cavities, Photonics, 8, 11, 2021, 470.
5. A. Laliwala, D. Svechkarev, M. R. Sadykov, J. Endres, K. W. Bayles, A.M. Mohs, Simpler procedure and improved performance for pathogenic bacteria analysis with a paper-based ratiometric fluorescent sensor array, Anal. Chem., 94, 5, 2022, 2615-2624.
6. C. Canto, $NAD^+$ Precursors: A Questionable Redundancy, Metabolites, 12, 7, 2022, 630.
7. T.S. Blacker, M. D. Sewell, G. Szabadkai, M.R. Duchen, Metabolic profiling of live cancer tissues using NAD(P)H fluorescence lifetime imaging, Cancer Metab.: Methods Protoc., 2019, 365-387.
8. A. Korkmaz, E. Arslan, M. Koşan, Volatile Compounds, Bioactive Properties and Chlorophylls Contents in Dried Spearmint (Mentha spicata L.) as Affected by Different Drying Methods, J. Agric. Sci., 29, 2, 2023, 604-617.
9. H. Kecis, Y. Abdelouahab, M. Bagues, L. Gali, F. Mekircha, W. Alloun, K. Nagaz, Phenolic profile and bioactivity of the aerial part and roots of Mentha rotundifolia L. grown in two different localities in northeastern Algeria: A comparative study, Biocatal. Agric. Biotechnol., 47, 2023, 102581.
10. L.L. Zhang, Y. Chen, Z.J. Li, X. Li, G. Fan, Bioactive properties of the aromatic molecules of spearmint (Mentha spicata L.) essential oil: A review, Food Funct., 13, 6, 2022, 3110-3132.
11. G. Mahendran, S. K. Verma, L. U. Rahman, The traditional uses, phytochemistry and pharmacology of spearmint (Mentha spicata L.): A review, J. Ethnopharmacol., 278, 2021, 114266.
12. J. Yang, P. Ju, X. Dong, J. Duan, H. Xiao, X. Tang, X. Zhai, B. Hou, Green synthesis of functional metallic nanoparticles by dissimilatory metal-reducing bacteria "Shewanella": A comprehensive review, J. Mater. Sci. Technol., 2023.
13. D. Jiang, D. Ni, Z.T. Rosenkrans, P. Huang, X. Yan, W. Cai, Nanozyme: new horizons for responsive biomedical applications, Chem. Soc. Rev., 48, 14, 2019, 3683-3704.
14. K. Wang, C. Han, J. Li, J. Qiu, J. Sunarso, S. Liu, The mechanism of piezocatalysis: energy band theory or screening charge effect? Angew. Chem., 134, 6, 2022, e202110429.
15. A. Das, M. T. Prabhu, N. Sarkar, Synthesis, characterization, and in vitro DPPH radical scavenging assay study of PEG-capped carbon nanoparticles derived from Butea monosperma flower extract, Adv. Nat. Sci.: Nanoscience Nanotechnol., 13, 1, 2022, 015002.
16. R.S. Dangana, R. C. George, F.K. Agboola, The biosynthesis of zinc oxide nanoparticles using aqueous leaf extracts of Cnidoscolus aconitifolius and their biological activities, Green Chem. Lett. Rev., 16, 1, 2023, 2169591.
17. W. Susmayanti, A. Rahmadani, Uji Aktivitas Antioksidan Fraksi Daun Melinjo (Gnetum Gnenom L.) Menggunakan Metode CUPRAC (Cupric Ion Reducing Antioxidant Capacity): Antioxidant Activity of Fraction From Gnetum Gnenom L. Leaves Using Cuprac (Cupric Ion Reduxing Antioxidant Capacity) Methods, Indones. J. Pharm. Nat. Prod., 6, 01, 2023, 97-106.
18. X. Huang, I.H. El-Sayed, X. Yi, M.A. El-Sayed, Gold nanoparticles: Catalyst for the oxidation of NADH to $NAD^+$, J. Photochem. Photobiol. B: Biol., 81, 2, 2005, 76-83.
19. E. Gallardo-Toledo, A. Tapia-Arellano, F. Celis, T. Sinai, M. Campos, M. J. Kogan, A.C. Sintov, Intranasal administration of gold nanoparticles designed to target the central nervous system: fabrication and comparison between nanospheres and nanoprisms, Int. J. Pharm., 590, 2020, 119957.
20. H.F. McMurdie, M.C. Morris, E. H. Evans, B. Paretzkin, W. Wong-Ng, L. Ettlinger, C.R. Hubbard, Standard X-ray diffraction powder patterns from the JCPDS research associateship, Powder Diffr., 1, 2, 1986, 64-77.
21. S. Fatimah, R. Ragadhita, D.F. Al Husaeni, A.B. Nandiyanto, How to calculate crystallite size from x-ray diffraction (XRD) using Scherrer method, ASEAN J. Sci. Eng., 2, 1, 2022, 65-76.
22. P. Jiang, Y. Wang, L. Zhao, C. Ji, D. Chen, L. Nie, Applications of gold nanoparticles in non-optical biosensors, Nanomaterials, 8, 12, 2018, 977.
23. A. Carone, S. Emilsson, P. Mariani, A. Désert, S. Parola, Gold nanoparticle shape dependence of

colloidal stability domains, Nanoscale Adv., 5, 7, 2023, 2017-2026.
24. Ü. Erdoğan, Ö. Özmen, M. Özer, Wound Healing, Anti-analgesic, and Antioxidant Activity of Nigella sativa Linn., Essential Based Topical Formulations in Rat Model Experimental Skin Defects, J. Essential Oil Bearing Plants, 2023, 1-6.
25. A.K. Mishra, K.N. Tiwari, R. Saini, J.K. Chaurasia, S.K. Mishra, Assessment of antioxidant potential in seed extracts of Nyctanthes arbor-tristis L. and phytochemical profiling by Gas Chromatography-Mass Spectrometry system, Braz. J. Pharm. Sci., 58, 2023.
26. A. Soni, M.P. Bhandari, G.K. Tripathi, P. Bundela, P.K. Khiriya, P.S. Khare, M.K. Kashyap, A. Dey, B. Vellingiri, S. Sundaramurthy, A. Suresh, Nano-biotechnology in tumour and cancerous disease: A perspective review, J. Cell. Mol. Med., 2023.
27. W.M. Aboulthana, E. Refaat, S.E. Khaled, N.E. Ibrahim, A.M. Youssef, Metabolite Profiling and Biological Activity Assessment of Casuarina equisetifolia Bark after Incorporating Gold Nanoparticles, Asian Pac. J. Cancer Prev., 23, 10, 2022, 3457-3471.
28. P. Jadczak, D. Kulpa, R. Drozd, W. Przewodowski, A. Przewodowska, Effect of AuNPs and AgNPs on the antioxidant system and antioxidant activity of lavender (Lavandula angustifolia Mill.) from in vitro cultures, Molecules, 25, 23, 2020, 5511.
29. G. Das, S. Seo, I.J. Yang, L. T. Nguyen, H. S. Shin, J.K. Patra, Synthesis of Biogenic Gold Nanoparticles by Using Sericin Protein from Bombyx mori Silk Cocoon and Investigation of Its Wound Healing, Antioxidant, and Antibacterial Potentials, Int. J. Nanomedicine, 2023, 17-34.
30. C. Hano, B.H. Abbasi, Plant-based green synthesis of nanoparticles: Production, characterization and applications, Biomolecules, 12, 1, 2021, 31.
31. S.J. Amina, B. Guo, A review on the synthesis and functionalization of gold nanoparticles as a drug delivery vehicle, Int. J. Nanomedicine, 2020, 9823-9857.
32. D. Vilela, M. C. González, A. Escarpa, Nanoparticles as analytical tools for in-vitro antioxidant-capacity assessment and beyond, TRAC Trends Anal. Chem., 64, 2015, 1-6.
33. A. Devadoss, L. Dennany, C. Dickinson, T. E. Keyes, R.J. Forster, Highly sensitive detection of NADH using electrochemiluminescent nanocomposites, Electrochem. Commun., 19, 2012, 43-45.
34. M. Jiang, L. Zhang, L. Liang, M.R. Khedri, Physico-chemical characterization and anti-laryngeal cancer effects of the gold nanoparticles, Arab. J. Chem., 2023, 104545.
35. G. Darabdhara, M.R. Das, S.P. Singh, A.K. Rengan, S. Szunerits, R. Boukherroub, Ag and Au nanoparticles/reduced graphene oxide composite materials: synthesis and application in diagnostics and therapeutics, Adv. Colloid Interface Sci., 271, 2019, 101991.
36. H. Aldewachi, T. Chalati, M.N. Woodroofe, N. Bricklebank, B. Sharrack, P. Gardiner, Gold nanoparticle-based colorimetric biosensors, Nanoscale, 10, 1, 2018, 18-33.
37. I. El-Sayed, X. Huang, F. Macheret, J.O. Humstoe, R. Kramer, M. El-Sayed, Effect of plasmonic gold nanoparticles on benign and malignant cellular autofluorescence: a novel probe for fluorescence based detection of cancer, Technol. Cancer Res. Treat., 6, 5, 2007, 403-412.
38. P. Fischer, J. Fleckenstein, J.O. Hönes, Spectroscopic investigation of dihydronicotinamides-I: conformation, absorption, and fluorescence, Photochem. Photobiol., 47, 2, 1988, 193-199.